Journal of Magnetic Resonance **153,** 75–82 (2001)
doi:10.1006/jmre.2001.2417, available online at http://www.idealibrary.com on IDEAL®

Improved Measurement of $^3J(H_i^\alpha, N_{i+1})$ Coupling Constants in H_2O Dissolved Proteins

Frank Löhr*,[1], Jürgen M. Schmidt,‡ Steffen Maurer,* and Heinz Rüterjans*

*Institut für Biophysikalische Chemie, Johann Wolfgang Goethe-Universität Frankfurt, Biozentrum N230, Marie Curie-Strasse 9, 60439 Frankfurt am Main, Germany; and ‡Division of Molecular Structure, National Institute for Medical Research, Mill Hill, London NW7 1AA, United Kingdom

E-mail: murph@bpc.uni-frankfurt.de

Received April 12, 2001; revised July 17, 2001; published online October 5, 2001

A modification to the recently proposed α/β-HN(CO)CA-*J* TROSY pulse sequence (P. Permi *et al., J. Magn. Reson.* 146, 255–259 (2000)) makes it possible to determine $^3J(H_i^\alpha, N_{i+1})$ coupling constants from a single E.COSY-type cross-peak pattern rather than from two $^1H^\alpha$ spin-state-edited subspectra. Advantages are increased ^{15}N resolution, critical to extracting accurate $^1H^\alpha$–^{15}N coupling constants, and minimized differential relaxation due to nested $^{13}C^\alpha$ and ^{15}N evolution periods. Application of the improved pulse sequence to *Desulfovibrio vulgaris* flavodoxin results in $^3J(H_i^\alpha, N_{i+1})$ values being systematically larger than those obtained with the original scheme. Parametrization of the coupling dependence on the protein backbone torsion angle ψ yields the Karplus relation $^3J(H_i^\alpha, N_{i+1}) = -1.00\cos^2(\psi - 120^\circ) + 0.65\cos(\psi - 120^\circ) - 0.15$ Hz, with a residual root-mean-square difference of 0.13 Hz between measured and back-calculated coupling constants. The curve compares with data derived from ubiquitin (A. C. Wang and A. Bax, *J. Am. Chem. Soc.* 117, 1810–1813 (1995)), although spanning a slightly larger range of *J* values in flavodoxin. The orientation of the Ala39/Ser40 peptide link, forming a type-II β-turn in flavodoxin, is twisted against X-ray-derived torsions by approximately 10° in the NMR structure as evident from the analysis of ϕ- and ψ-related ^3J coupling constants. The remaining deviation of some experimental values from the prediction is likely to be due to strong hydrogen bonding, substituent effects, or the additional dependence on the adjacent torsions ϕ. © 2001 Academic Press

Key Words: **ψ-angle; E.COSY; flavodoxin; hydrogen bonds; TROSY.**

INTRODUCTION

Scalar three-bond couplings between polypeptide α-protons and amide nitrogens of the subsequent residue, owing to their dependence on the ψ torsion angle (*1–8*), are indicative of backbone conformation. Empirical parametrization of the corresponding Karplus relation using ubiquitin data referencing crystal coordinates (*9*) revealed that the range of $^3J(H_i^\alpha, N_{i+1})$ coupling constants in proteins is considerably smaller than originally anticipated. This makes highly accurate and precise measurements all the more critical for deriving useful angular restraints for protein-structure determination.

Pioneering studies on $^3J(H_i^\alpha, N_{i+1})$ in proteins exploited the splitting fine structure of $^1H_i^\alpha$–$^1H_{i+1}^N$ multiplets in ^{15}N-coupled NOESY spectra (*10,11*) in an E.COSY fashion (*12*). While recording such spectra is straightforward, signal overlap, large variations in signal intensities, and interference from the residual solvent signal in the α-proton region may severely limit the analysis. In a different approach, the size of the scalar $^1H_i^\alpha$–$^{15}N_{i+1}$ interaction has been encoded in cross-peak intensities for quantitative evaluation (*13*), using the HNHB pulse sequence (*14–17*), originally designed to measure intraresidue $^1H^\beta$–^{15}N coupling constants. Apparently, this method suffers from the small intrinsic magnitude of $^3J(H_i^\alpha, N_{i+1})$ couplings. Both problems, signal overlap and low sensitivity, are avoided with the HCACO[N]-E.COSY method (*9*) in which magnetization transfer relies exclusively on one-bond scalar couplings giving rise to a single cross peak per residue. In larger proteins, however, the $^{13}C'$ linewidth often exceeds the size of the auxiliary $^1J(C_i', N_{i+1})$ coupling (≈15 Hz), exploited to separate E.COSY-multiplet components in the orthogonal $^{13}C'$ dimension, resulting in a nonresolved $^3J(H_i^\alpha, N_{i+1})$ doublet, thus compromising its accurate determination.

Alternatively, the HCA(CO)N-*J* pulse scheme (*18*) takes advantage of the substantially larger $^1J(C_i^\alpha, H_i^\alpha)$ interaction (≈140 Hz) for separating E.COSY-multiplet constituents and provides the desired coupling constants in the indirectly detected ^{15}N dimension. The drawback of the latter two methods is the demand for $^{13}C/^{15}N$ doubly labeled protein samples that must be dissolved in D_2O. In contrast, while sharing the E.COSY-like cross-peak pattern with the HCA(CO)N-*J*, the HN(CO)CA-*J* (*19*) detects amide protons, allowing protein spectra to be recorded in H_2O solution. In an improved version, the HN(CO)CA-*J* approach (*20*) elegantly combines the advantages of TROSY-type ^{15}N and $^1H^N$ evolution (*21–25*) and spin-state-selective polarization (*26*), to edit $^{13}C^\alpha$–$^1H^\alpha$

[1] To whom correspondence should be addressed. Fax: +49-69-798-29632.

1090-7807/01 $35.00

doublet components into two subspectra. Incorporation of the TROSY technique not only ensures enhanced sensitivity and resolution, but also avoids $^1H^N$ band-selective inversion during ^{15}N evolution of the original pulse scheme (*19*), which might perturb supposedly passive $^1H^\alpha$ spin states and result in incomplete decoupling of $^1J(^{15}N,^1H)$ interactions.

Both α/β-HN(CO)CA-*J* TROSY and HCACO[N]-E.COSY experiments applied to ubiquitin revealed no significant differences in the $^3J(H_i^\alpha, N_{i+1})$ values measured (*9, 20*). However, in all but the fastest tumbling proteins, passive $^1H^\alpha$ spin flips, inevitable in the interval between $^{13}C^\alpha$ and ^{15}N evolution times of the HN(CO)CA-*J*, give rise to additional small E.COSY-like doublets of opposite tilt. In the multiplet they are not resolvable but result in an apparent displacement of the two main components toward their center in the ^{15}N dimension and thereby to an underestimation of $^3J(H_i^\alpha, N_{i+1})$ coupling constants (*27, 28*). Clearly, it would be desirable to shorten the duration needed for relayed polarization transfer between $^{13}C^\alpha$ and ^{15}N. Here, we present a modified version of the HN(CO)CA-*J* TROSY to obtain E.COSY-type multiplets void of such differential-relaxation effects, therefore providing for more accurate $^3J(H_i^\alpha, N_{i+1})$ coupling constants.

RESULTS AND DISCUSSION

In order to determine protein backbone torsion angles ψ, two-dimensional α/β-HN(CO)CA-*J* TROSY (*20*) has been applied to oxidized *Desulfovibrio vulgaris* flavodoxin. The magnitudes of $^3J(H_i^\alpha, N_{i+1})$ couplings measured fell appreciably short of expectations from a Karplus curve by Wang and Bax (*9*) derived for ψ torsion angles on the basis of ubiquitin crystal coordinates. Being of molecular mass of 16.3 kDa, flavodoxin is approximately twice as large as ubiquitin. Permi and co-workers (*20*) proposed to alleviate the problem of underestimating $^3J(H_i^\alpha, N_{i+1})$ due to differential relaxation in larger proteins by decreasing the interval between the $^1H^\alpha$ spin-state-selective filter and the ^{15}N evolution period, denoted $2T_b$ in their pulse sequence, usually adjusted to $1/(2^1J_{C\alpha C'})$. In practice, the 114 *J* coupling constants in flavodoxin repeatedly taken at $2T_b = 7$ ms are highly reproducible (pairwise rmsd of 0.09 Hz in two experiments), yet a pronounced dependence on the actual setting of T_b was observed. The shorter this period during which $^1H^\alpha$ spin flips occur, the larger the absolute value of the apparent coupling constants, as illustrated in Fig. 1, lending to believing measuring true $^3J(H_i^\alpha, N_{i+1})$ coupling constants would require T_b be minimized or not present at all. Seriously limiting this approach, a shorter T_b trades in sensitivity for accuracy as cross-peak intensities scale back due to their dependence on $\sin(^1J_{C\alpha C'}\pi 2T_b)$.

The 3D [^{15}N,^1H]-TROSY-HN(CO)CA[HA]-E.COSY pulse sequence we propose avoids any delay between $^{13}C^\alpha$ and ^{15}N evolution periods, thus decreasing the chance of differential-relaxation effects. The scheme outlined in Fig. 2 is closely related to the original α/β-HN(CO)CA-*J* TROSY experiment, so we can refer to the detailed description already given in Ref. (*20*).

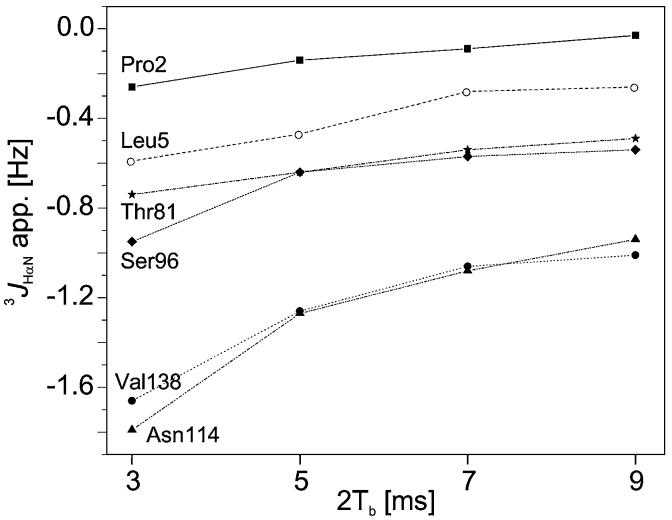

FIG. 1. Experimental dependence of apparent $^3J(H_i^\alpha, N_{i+1})$ coupling constants on the duration of the $C^\alpha \rightarrow C'$ back transfer period, $2T_b$, in a series of 2D α/β-HN(CO)CA-*J* TROSY multiplets (*20*) for selected residues in *Desulfovibrio vulgaris* flavodoxin.

Importantly, the modified coherence transfer between $^{13}C_i^\alpha$ and $^{15}N_{i+1}$ is achieved via a $^{13}C'$-relayed HMQC module (*43, 44*), rather than using successive $^{13}C_i^\alpha - ^{13}C_i'$ and $^{13}C_i' - ^{15}N_{i+1}$ INEPT (*45*) steps on the single-quantum level. Thus, during t_2, the desired magnetization evolves as $^{13}C_i^\alpha$, $^{15}N_{i+1}$ multiple-quantum coherence antiphase with respect to $^1J_{C\alpha C'}$ and $^1J_{NH}$. Note that the effect of nitrogen-chemical shift evolution in t_2 is negated by appropriate displacement of the ^{15}N 180° pulses between periods T_N^a and T_N^b. Furthermore, in our pulse sequence the $^1H^\alpha$ spin-state-selective filter is omitted, and *J* scaling in the $^{13}C^\alpha$ evolution time is not employed, resulting in a conventional E.COSY multiplet pattern (*10–12*) with the two components corresponding to the α- and β-spin states of $^1H^\alpha$ appearing in a single spectrum. It should be noted that the relayed HMQC-type $^{15}N_{i+1} - ^{13}C_i^\alpha$ correlation scheme precludes the application of proton inversion pulses during periods of transverse $^{13}C^\alpha$ magnetization because of inevitable modulations due to $^1J_{NH}$ interactions. The approach proposed here is therefore incompatible with both the $^1H^\alpha$ spin-state-selective filter and *J* scaling in t_2 as employed in the α/β-HN(CO)CA-*J* TROSY experiment (*20*).

Our concept offers the advantage of a prolonged ^{15}N evolution period t_1 as use can be made of the durations δ and ε, flanking the central t_2 evolution time and totalling 84 ms, required for the magnetization transfer via $^1J_{NC'}$ and $^1J_{C'C\alpha}$ couplings, respectively (*46*). Extended to more than 170 ms in the present version, the ^{15}N acquisition mode may be referred to as double semiconstant-time or shared-time shift labeling (*47, 48*) (for details see the legend to Fig. 2). Combined with TROSY-type selection of the slower relaxing ^{15}N component, this results in a highly resolved ω_N frequency domain critical to accurate extraction of the comparatively small $^3J(H_i^\alpha, N_{i+1})$ coupling constants. In addition, the shared ^{15}N and $^{13}C^\alpha$ evolution time renders

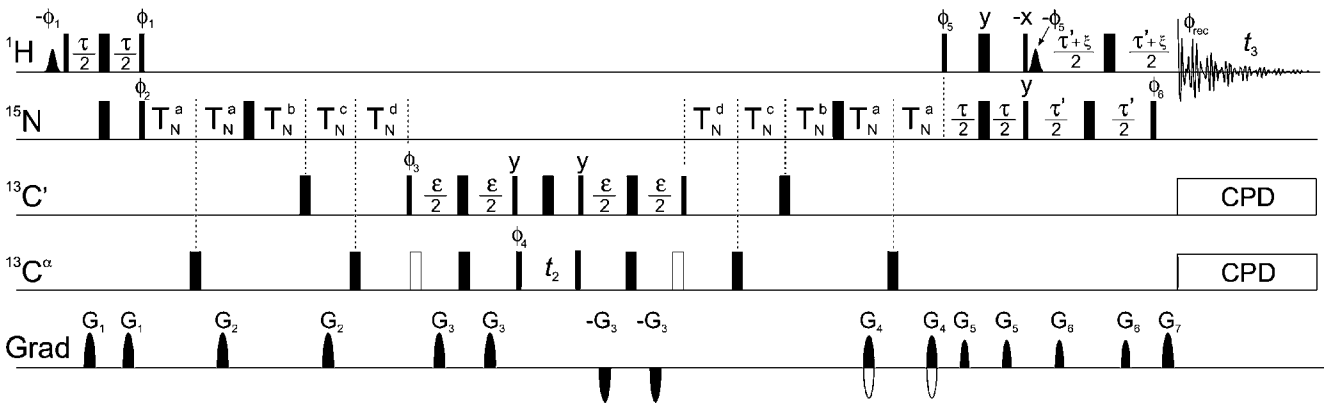

FIG. 2. Pulse scheme of the 3D [^{15}N,^{1}H]-TROSY-HN(CO)CA[HA]-E.COSY experiment. Narrow and wide bars denote RF pulses with flip angles of 90° and 180°, respectively, applied along the x axis unless specified. All proton pulses are centered at the water resonance (4.75 ppm). The two Gaussian-shaped pulses (duration 2 ms, truncation level 10%) ensure alignment of the water magnetization along the positive z axis to avoid saturation of fast-exchanging amide protons (*29–31*). Carrier frequencies for ^{15}N and ^{13}C pulses are positioned at 119 and 56.5 ppm, respectively. Pulses applied to α-carbons are rectangular and employ RF fields of $\Delta/\sqrt{15}$ (90° flip angle) or $\Delta/\sqrt{3}$ (180° flip angle), where Δ is the difference (in Hz) between the centers of the $^{13}C^\alpha$ and $^{13}C'$ resonance regions (*32*). Pulses inserted to compensate Bloch–Siegert phase shifts on $^{13}C'$ are represented by open rectangles. Carbonyl-selective 90° and 180° pulses (duration 124 μs at 150.9 MHz ^{13}C frequency) are applied at 176.5 ppm using phase modulation (*33, 34*) and have an amplitude envelope corresponding to the center lobe of a $\sin(x)/x$ function. The carbonyl pulse in the center of t_2 is cosine-modulated to provide two excitation maxima at ±120 ppm from the ^{13}C carrier position, thus avoiding Bloch–Siegert-like effects on α-carbons (*35*). During acquisition, proton–carbon long-range couplings are eliminated by a sequence of 3-ms WURST-20 (*36*) pulses (50 kHz sweep) centered at 106 ppm and employing a five-step supercycle (*37*). The periods for de- and rephasing due to ^{15}N–$^{13}C'$ and $^{13}C'$–$^{13}C^\alpha$ couplings are adjusted to $\delta = 33$ ms ($\approx 1/(2^1J_{NC'})$) and $\varepsilon = 9$ ms ($\approx 1/(2^1J_{C'C\alpha})$), respectively. The initial durations of T_N^a, T_N^b, T_N^c, and T_N^d are $(\delta+\varepsilon)/4$, 0, $(\delta-\varepsilon)/4$, and $(\delta-\varepsilon)/4$, respectively. Nitrogen-chemical shift evolution occurs in a semi-constant time manner (*38, 39*), where T_N^a is decremented while T_N^b, T_N^c, and T_N^d are incremented as a function of t_1. In addition, periods T_N^a, T_N^c, and T_N^d are altered in the opposite direction as a function of t_2 to avoid a modulation due to ^{15}N chemical shifts in the $^{13}C^\alpha$ domain, finally yielding $T_N^a = (\delta+\varepsilon)/4-\kappa t_1/8+t_2/8$; $T_N^b = (1-\kappa)t_1/4$; $T_N^c = (\delta-\varepsilon)/4+\kappa t_1/8-t_2/8$; $T_N^d = (\delta-\varepsilon)/4+(2-\kappa)t_1/8-t_2/8$, where the factor $\kappa = [2(\delta+\varepsilon)-\tau(G_2)]/t_{1,\max.}$ and $\tau(G_2)$ is the duration of gradient G_2 including recovery time. The fixed delays τ, τ', and ξ are set to 4.6, 5.4, and 0.4 ms, respectively. In order to constructively add components originating from ^{1}H and ^{15}N steady-state magnetization (*21, 40*), the pulse phase ϕ_1 is y on Bruker spectrometers while it must be inverted for applications on Varian spectrometers (*41*). Remaining phases are cycled according to $\phi_2 = y$; $\phi_3 = 2(x)$, $2(-x)$; $\phi_4 = x, -x$; $\phi_5 = y$; $\phi_6 = x$; $\phi_{\text{receiver}} = x, 2(-x), x$. Gradients are sine-bell shaped and have the following durations, peak amplitudes, and directions: G_1, 0.5 ms, 7.5 G/cm, x; G_2, 0.5 ms, 6 G/cm, y; G_3, 0.5 ms, 5 G/cm, z; G_4, 0.4 ms, 39.45 G/cm, xyz; G_5, 0.3 ms, −4 G/cm, xy; G_6, 0.3 ms, 5.5 G/cm, xy; G_7, 0.2 ms, 16 G/cm, xyz. For each t_1 increment N- and P-type transients are collected alternately by inverting the polarity of G_4 along with pulse phases ϕ_5 and ϕ_6. The two transients are stored separately and then added and subtracted to form the real and imaginary parts of a complex FID with a 90° zero-order phase shift being added to one of the components. Axial peaks in the ^{15}N dimension are shifted to the edge of the spectrum by incrementing ϕ_2 and the receiver phase by 180° for each value of t_1. Quadrature detection in t_2 is accomplished by altering ϕ_4 in the States–TPPI (*42*) manner.

ineffective the differential relaxation of those coherences in- and antiphase with respect to passive $^1H^\alpha$ spins causing systematic underestimation of $^3J(H_i^\alpha, N_{i+1})$. Unlike the delay $2T_b$ in the α/β-HN(CO)CA-J TROSY, the corresponding $^{13}C'$-relay period ε in [^{15}N, ^{1}H]-TROSY-HN(CO)CA[HA]-E.COSY, since forming part of the evolution period t_1, is not expected critically to affect the coupling constants.

Advantages of spin-state-selective polarization (S^3P) over E.COSY-type experiments are improved sensitivity and effective spectral resolution (*26*). In the concept of HN(CO)CA-J, resolution is gained as a result of editing the doublet components corresponding to α- and β-spin states of $^1H^\alpha$ in two subspectra. Sensitivity is enhanced, in principle, due to the fact that S^3P does not require complete resolution of the $^1J_{C\alpha H\alpha}$ splitting in the $^{13}C^\alpha$ dimension, where resonances are often broadened by fast transverse relaxation and passive $^1J_{C\alpha C\beta}$ and $^1J_{C\alpha N}$ couplings. It should however be noted that the $^{13}C^\alpha$ evolution time, which is additional to the editing delay of $(^1J_{C\alpha H\alpha})^{-1}$ in the 3D version of the α/β-HN(CO)CA-J TROSY, compromises the sensitivity advantage. In the case of the 147-residue protein flavodoxin, E. COSY spectra were recorded within less than a day experiment time with good signal-to-noise, and a virtually complete set of $^3J(H_i^\alpha, N_{i+1})$ coupling constants was obtained, so that [^{15}N, ^{1}H]-TROSY-HN(CO)CA[HA]-E.COSY experiments were not found to be limited by resolution or sensitivity issues. However, spectral overlap and signal decay in the $^{13}C^\alpha$ domain are likely to become more severe with larger proteins.

Representative cross peaks from a 3D spectrum obtained by application of the novel pulse sequence to flavodoxin are shown in Fig. 3. The principal multiplet components are located in (F_1, F_2, F_3) at positions ($\omega_{N(TR)} + \pi^3 J_{H\alpha N}$, $\omega_C + \pi^1 J_{C\alpha H\alpha}$, $\omega_{H(TR)}$) and ($\omega_{N(TR)} - \pi^3 J_{H\alpha N}$, $\omega_C - \pi^1 J_{C\alpha H\alpha}$, $\omega_{H(TR)}$), where $\omega_{N(TR)} = \omega_N - \pi^1 J_{NH}$, $\omega_{H(TR)} = \omega_H - \pi^1 J_{NH}$, and ω_N, ω_C, and ω_H are the Larmor frequencies of $^{15}N_{i+1}$, $^{13}C_i^\alpha$, and $^1H_{i+1}^N$. The sought vicinal coupling constant corresponds to the displacement of the two components along F_1. Quantitative evaluation of the spectra resulted in a set of 125 out of 126 possible (nonglycine) $^3J(H_i^\alpha, N_{i+1})$ coupling constants. Average values from five independent measurements are in the range from −0.05 to −2.14 Hz, in agreement with results reported

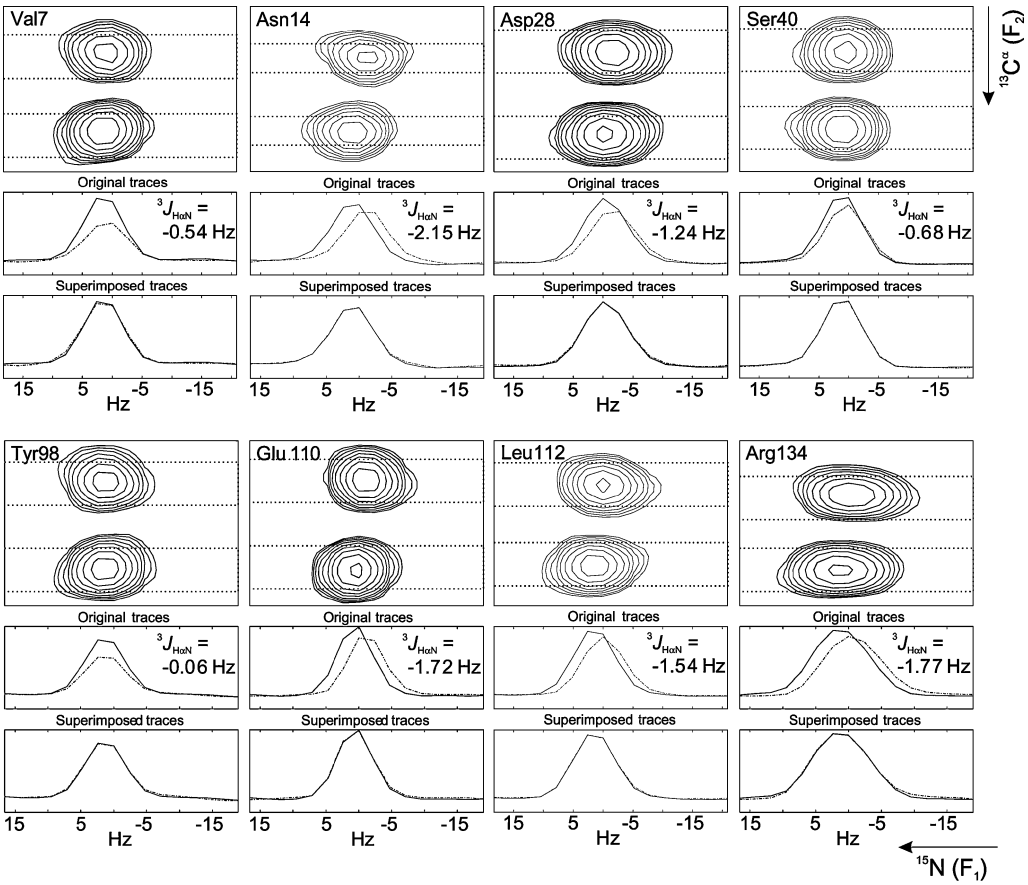

FIG. 3. Determination of $^3J(\mathrm{H}_i^{\alpha}, \mathrm{N}_{i+1})$ coupling constants from 3D [^{15}N,^{1}H]-TROSY- HN(CO)CA[HA]-E.COSY spectra of flavodoxin. The contour plots at the top of each panel show ^{15}N–$^{13}C^{\alpha}$ projections obtained by summing over three spectral points along F_3, centered around the $^1H^N$ chemical shift of the residue sequentially following the one indicated. Levels are drawn on an exponential scale using a factor of $2^{1/2}$. In the lower half of each panel, one-dimensional traces of the upfield (dot-dashed lines) and downfield (solid lines) multiplet halves, resulting from projections along F_2 with limits as indicated by dotted lines in the respective contour plots, are shown before and after fitting peak amplitudes and horizontal positions. Note that digital resolutions vary among the spectra and that the extracted J values are unaffected by the relatively coarse digitization in the ^{15}N dimension as the fit is carried out in the time domain.

by other groups (*9, 16, 18, 20*), but considerably smaller than data from Seip *et al.* (*19*), who found $^3J(\mathrm{H}_i^{\alpha}, \mathrm{N}_{i+1})$ interactions to be as strong as −6.5 Hz using the original version of the HN(CO)CA-*J* pulse sequence. The mean standard deviation for individual residues is 0.07 Hz, indicating a remarkably low random experimental error.

Cross-correlated relaxation taking place during the multiple-quantum evolution period t_2 causes a differential change of intensities between the two $^{13}C^{\alpha}$– $^1H^{\alpha}$ doublet lines. The effect is governed by dipolar (DD) relaxation interference between bond vectors $^{13}C_i^{\alpha}$–$^1H_i^{\alpha}$ and $^{15}N_{i+1}$–$^1H_{i+1}^{N}$ in proteins and depends on the intervening torsion angle ψ. It is most pronounced in the region around $\psi = +120^{\circ}$ (*49–51*), for example, for Val7 and Tyr98 (Fig. 3), where $^3J(\mathrm{H}_i^{\alpha}, \mathrm{N}_{i+1})$ couplings are small. Additional minor contributions may arise from various DD/DD mechanisms, such as vector pairs $^{13}C_i^{\alpha}$–$^1H_i^{\alpha}$/$^{13}C_i^{\alpha}$–$^1H_{i+1}^{\mathrm{N}}$, $^{13}C_i^{\alpha}$–$^1H_i^{\alpha}$/$^{15}N_{i+1}$–$^1H_i^{\alpha}$, $^{15}N_{i+1}$–$^1H_i^{\alpha}$/$^{15}N_{i+1}$–$^1H_{i+1}^{\mathrm{N}}$, and $^{13}C_i^{\alpha}$–$^1H_{i+1}^{\mathrm{N}}$/$^{15}N_{i+1}$–$^1H_i^{\alpha}$, and also from chemical shift anisotropy ascribed to ^{15}N or $^{13}C^{\alpha}$, giving rise to CSA/DD relaxation interference, like $^{13}C_i^{\alpha}$/$^{13}C_i^{\alpha}$–$^1H_i^{\alpha}$, $^{15}N_{i+1}$/$^{13}C_i^{\alpha}$–$^1H_i^{\alpha}$, $^{13}C_i^{\alpha}$/$^{15}N_{i+1}$–$^1H_i^{\alpha}$, and $^{15}N_{i+1}$/$^{15}N_{i+1}$–$^1H_i^{\alpha}$. However, since these interactions do not change the ^{15}N resonance positions of the doublet components, measurement of the desired scalar coupling constants remains unaffected. In contrast, CSA/DD cross-correlated relaxation of the two coupled nuclei may result in dynamic frequency shifts, which would be indistinguishable from J couplings in the experiments applied here (*52, 53*). Given the relatively large $^{15}N_{i+1}$–$^1H_i^{\alpha}$ distance, however, their dipolar interaction is weak and the contribution of dynamic frequency shifts to the measured splittings should fall below the experimental precision. For the same reason residual dipolar couplings, caused by a partial orientation of the molecule in the magnetic field, are not expected to exceed ≈0.02 Hz for the diamagnetic protein studied here (*53*).

A comparison between J values obtained with the S^{3}P and E.COSY versions of the HN(CO)CA-*J* TROSY experiment is presented in Fig. 4. While precision of the two data sets is comparable and the correlation coefficient is $R = 0.97$, linear regression yields a slope of 1.39, indicating that α/β-HN(CO)CA-*J*

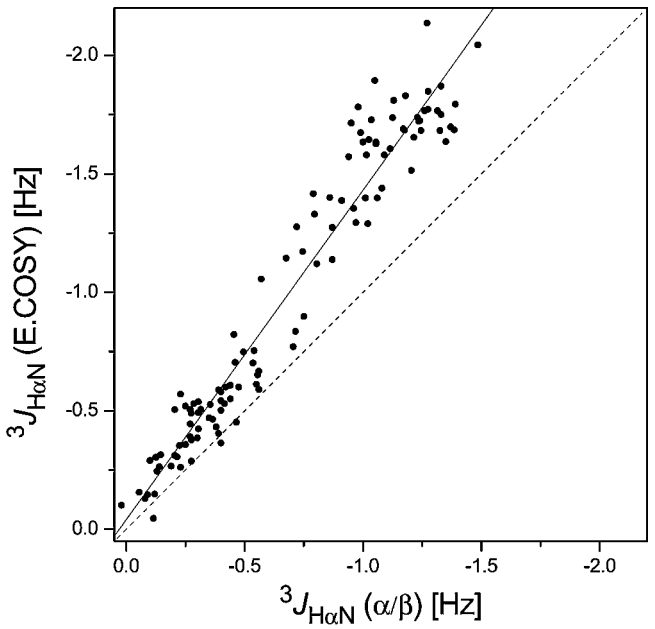

FIG. 4. Comparison of $^3J(H_i^\alpha, N_{i+1})$ coupling constants measured for flavodoxin using the new 3D [^{15}N, ^{1}H]-TROSY-HN(CO)CA[HA]-E.COSY pulse sequence and the reference 2D α/β-HN(CO)CA-J TROSY experiment (*20*). J values represent averages from two spectra recorded with $2T_b = 7$ ms and from five spectra, respectively. The continous line shows the result of a linear regression.

TROSY as applied to flavodoxin results in a severe reduction of the observed $^3J(H_i^\alpha, N_{i+1})$ coupling constants.

The coupling constants measured with the E.COSY-type pulse sequence differ by 0.14 Hz (rmsd) from the ubiquitin-derived Karplus relation given by Wang and Bax (*9*), $^3J(H_i^\alpha, N_{i+1}) = -0.88\ \cos^2(\psi - 120^\circ) + 0.61\cos(\psi - 120^\circ) - 0.27$ Hz. To assess the accuracy of these data, coupling constants were correlated with ψ angles in the X-ray structure (0.17 nm resolution) of oxidized flavodoxin (*54, 55*) (Fig. 5), although it should be kept in mind that static differences between solution and solid states as well as angular motional averaging can give rise to apparent deviations from the expected dihedral-angle dependence (*56*). However, ^{15}N relaxation measurements (*57*) and self-consistent analysis of ϕ-angle related ^3J coupling constants (*58*) revealed uniform and low flexibility in the backbone of oxidized flavodoxin, suggesting that the new Karplus curve is barely affected by motional averaging. Including the entire set of 125 coupling constants, reparametrization of the Karplus relation with flavodoxin X-ray data improves the rmsd$_J$ to 0.13 Hz, yielding Karplus coefficients $A = -1.00$, $B = +0.65$, $C = -0.15$, exhibiting a spread between minima and maxima larger than that found in earlier studies (*9*).

The two extreme $^3J(H_i^\alpha, N_{i+1})$ values in the graph of Fig. 5 deserve closer inspection. They are assigned to $^1H_i^\alpha$ of Thr11 (-2.04 ± 0.03 Hz) and Asn14 (-2.14 ± 0.09 Hz), adjacent to which amide nitrogens N_{i+1}, i.e., of residues Thr12 and Thr15, are involved in strong hydrogen bonds to the phosphate group of the flavin mononucleotide cofactor, as evidenced by through-hydrogen bond $^{3h}J_{NP}$ and/or $^{2h}J_{HP}$ couplings (*59*). This suggests that hydrogen bonding can have an influence on scalar $^1H_i^\alpha$–$^{15}N_{i+1}$ coupling constants, possibly through small changes of bond lengths and bond angles.

Another feature is that only 2 of the 17 couplings to glycine nitrogens coincide with the Karplus curve of Wang and Bax (*9*), whereas the remaining 15 are significantly displaced toward 0. This observation may hint to substituent effects, in line with previous experience with $^3J(H_i^\alpha, N_{i+1})$ couplings to proline nitrogens in ubiquitin (*9*) and with χ1-related ^3J couplings in flavodoxin (*60*). Unfortunately, HN(CO)CA-J type experiments are incapable of providing data for prolines lacking the amide proton. Excluding from the Karplus parametrization all residues preceding glycines as well as Thr11 and Asn14 results in only minor changes of the coefficients ($A = -0.97$, $B = +0.65$, $C = -0.18$) while diminishing the rmsd$_J$ to 0.12 Hz.

Overall, the present data indicate that $^3J(H_i^\alpha, N_{i+1})$ coupling constants primarily depend on the backbone torsion angle ψ. However, a few data points other than those mentioned above still deviate from the corresponding Karplus relation, while a simple explanation cannot be given. The largest discrepancy between observed coupling constants and predictions based on our Karplus parameters amounts to 0.47 Hz and is found for Ala39, where $^3J(H_i^\alpha, N_{i+1}) = -1.12 \pm 0.09$ Hz. Interestingly, in the X-ray structure, the backbone conformations of residues Ala39 and Ser40 in flavodoxin form a type-II β-turn, showing $(\phi_i, \psi_i, \phi_{i+1}, \psi_{i+1}) = (-58^\circ, -37^\circ, -94^\circ, +14^\circ)$, deviating only slightly from ideal turn-II geometry ($-60^\circ, -30^\circ$,

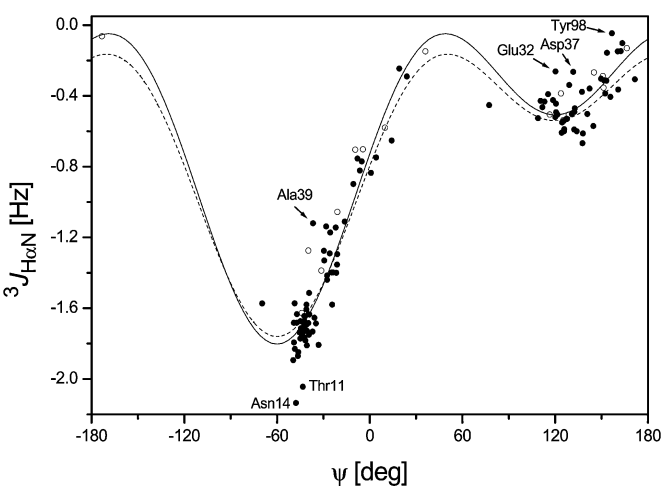

FIG. 5. Dependence of $^3J(H_i^\alpha, N_{i+1})$ coupling constants in oxidized *Desulfovibrio vulgaris* flavodoxin on crystallographic torsion angles ψ_i (*54, 55*). Open and closed circles denote data for glycine and nonglycine residues $i + 1$, respectively. The dashed line represents the Karplus curve of Ref. (*9*) and the continuous line corresponds to $^3J(H_i^\alpha, N_{i+1}) = -1.00\ \cos^2(\psi - 120^\circ) + 0.65\cos(\psi - 120^\circ) - 0.15$ Hz, obtained by fitting to the present data. Residues discussed in the text are indicated.

$-90°$, $0°$). Thorough analysis of ϕ-related ^3J coupling constants (*58*) revealed minor but significant differences in the NMR structure of the backbone stretch near Ala39 and Ser40 with $\phi_i = -67°$ and $\phi_{i+1} = -105°$, respectively. Possibly, the assumption of NMR and X-ray structures being identical does not hold for this portion of the protein. It is likely that the unexpected coupling constant observed reflects precisely this different orientation of the Ala39/Ser40 peptide link in the NMR structure. Perhaps, rather than with the X-ray derived torsion value, the data point belonging to Ala39 in Fig. 5 should have been associated with the—yet unknown—NMR-based ψ_i torsion value, likely to be offset by as big a difference as the adjacent torsion ϕ_{i+1}, of opposite sign though, coming close to $-26°$ instead of $-37°$. As ^3J varies quite steeply with the angle in the respective range, the match between experimental and back-calculated coupling constants would improve considerably.

More speculative, $^3J(H_i^\alpha, N_{i+1})$ coupling constants can be sensitive to the ϕ torsion angle too, as already suggested by DeMarco *et al.* (*7*), a notion supported by calculations based on density-functional theory, predicting $^3J(H_i^\alpha, N_{i+1})$ couplings in dipeptides to vary with ϕ by as much as 0.7 Hz (*61*). Such a variation is possibly reflected in the observed J values of residues Glu32 (-0.26 ± 0.01 Hz, $\phi_i = -94°$, $\psi_i = +120°$), Asp37 (-0.26 ± 0.06 Hz, $\phi_i = -67°$, $\psi_i = +132°$), and Tyr98 (-0.05 ± 0.05 Hz, $\phi_i = -88°$, $\psi_i = +157°$), whose backbone conformations differ from those of the majority of residues in flavodoxin, belonging to regular α-helical or β-sheet secondary structure elements. Coupling constants deviate from the values back-calculated on the basis of our Karplus parameters by 0.25, 0.22, and 0.23 Hz, respectively, clearly exceeding experimental precision. Since, in contrast to the case of Ala39, the corresponding data points fall in a relatively flat region of the Karplus curve (Fig. 5), it appears unlikely that deviations of the adjacent ψ angles in solution and in the crystal or J-averaging due to increased conformational flexibility alone account for the discrepancy.

CONCLUSIONS

We have proposed an improved version of the HN(CO)CA-J experiment, designated [^{15}N, ^{1}H]-TROSY-HN(CO)CA[HA]-E.COSY, which allows more accurate measurements of $^3J(H_i^\alpha, N_{i+1})$ coupling constants in proteins. Systematic diminuation of J as caused by passive $^1H^\alpha$ spin flips during critical transfer periods between the indirect detection periods is avoided by a multiple-quantum ^{15}N–$^{13}C^\alpha$ correlation scheme. Overall, the coupling constants measured in flavodoxin agree with ψ angles from X-ray data. In some cases more subtle effects like hydrogen bonding, substituents, and ϕ angles are likely to have an influence on the values observed. The pulse sequence proposed may offer an experimental basis to study such factors, yet more comprehensive investigations are beyond the scope of this paper.

EXPERIMENTAL

All experiments were carried out using a 1.4 mM sample of ^{13}C/^{15}N-labeled *Desulfovibrio vulgaris* flavodoxin dissolved in 0.5 ml 10 mM potassium phosphate buffer (pH 7) containing 5% D_2O. Spectra were recorded on Bruker Avance spectrometers operating at ^{1}H resonance frequencies of 600.13 and 800.13 MHz, using 5-mm three-axis gradient ^{1}H{^{13}C, ^{15}N}-triple-resonance probes. The temperature was adjusted to 27°C.

TABLE 1
Acquisition Parameters for α/β- and E.COSY-Type HN(CO)CA-J Experiments for the Determination of $^3J(H_i^\alpha)$, N_{i+1})

Experiment		Time domain points		Spectral widths		Acquisition times			
Type	$2T_b$ (ms)	t_1 (^{15}N) (complex)	t_2 ($^{13}C^\alpha$) (complex)	F_1 (^{15}N) (ppm)	F_2 ($^{13}C^\alpha$) (ppm)	t_1 (^{15}N) (ms)	t_2 ($^{13}C^\alpha$) ms	Scans per FID	Time[a] (h)
α/β[b]	9	512	n.a	28.3	n.a	223.0	n.a	8	10
	7	512	n.a	28.3	n.a	223.0	n.a	8	10
	7	512	n.a	28.3	n.a	223.0	n.a	8	7
	5	512	n.a	28.3	n.a	223.0	n.a	16	12
	3	512	n.a	28.3	n.a	223.0	n.a	16	14
E.COSY[c]	n.a	112	20	10.0	12.0	184.6	11.0	4	17
	n.a	128	19	12.0	10.0	176.1	12.6	4	20
	n.a	124	20	11.0	11.0	185.5	12.0	4	20
	n.a.	128	19	10.0	10.0	211.0	12.6	4	21
	n.a.	148	28	18.1	14.7	164.6	10.1	4	24

Note. n.a., not applicable.
[a] Total recording time for pairs of 2D in- and antiphase (α/β) or single 3D (E.COSY) spectra.
[b] Recorded with the 2D α/β-HN(CO)CA-J TROSY pulse sequence (*20*).
[c] Recorded with the present 3D [^{15}N,^{1}H]-TROSY-HN(CO)CA[HA]-E.COSY pulse sequence.

A 2D version of the α/β-HN(CO)CA-J TROSY experiment, derived from the pulse sequence in Ref. (*20*) by omitting the C^α evolution period, was repeated five times, using durations of the second $2T_b$ interval of 9, 7 (2×), 5, and 3 ms. Spectra were acquired at 800 MHz with 1280 complex points, corresponding to an acquisition time of 106.5 ms at a spectral width of 15.0 ppm in the proton dimension. Nitrogen chemical shifts were sampled in a semi-constant time manner using a factor κ of 0.13. The 3D [^{15}N, ^{1}H]-TROSY-HN(CO)CA[HA]-E.COSY experiment of Fig. 2 was performed five times at 600 MHz ^{1}H frequency using variable spectral widths in the F_1 (^{15}N) and F_2 (^{13}C) dimensions to account for accidental overlap of aliased and unaliased cross peaks. The ^{1}H spectral width was uniformly set to 14.7 ppm with an acquisition time adjusted to 87.3 ms (768 complex data points). Semi-constant time factors κ varied between 0.37 and 0.45, depending on ^{15}N acquisition times. Further details on acquisition parameters are listed in Table 1.

Spectra were processed using Bruker Xwin-nmr software. Prior to Fourier transformation, both ^{1}H and ^{15}N time domain data were apodized with squared-cosine functions. Using linear prediction, ^{13}C acquisition data of 3D spectra were extended by 30% and then weighted with a 60° shifted sine-bell function. Zero-filling was applied to obtain final 2D and 3D data set sizes of 1024 × 2048 and 256 × 64 × 1024 (512 × 128 × 1024 for the last entry in Table 1) real points, respectively, retaining only the low-field half in the ^{1}H dimension. Typically, the digital resolution in the ^{15}N dimension was 2.2 to 2.8 Hz/point. $^3J(H_i^\alpha, N_{i+1})$ coupling constants were analyzed from a pair of F_1 traces generated by summing over appropriate multiplet sections in F_2 (2D spectra) or F_2 and F_3 (3D spectra). The displacement of the two multiplet components along this dimension was found by a trace-alignment procedure involving FT-based time-domain convolution and least-squares superposition (*62*).

ACKNOWLEDGMENTS

This work was supported by a grant from the Deutsche Forschungsgemeinschaft (Ru 145/14-1). We thank Professor S. G. Mayhew (Department of Biochemistry, University College Dublin) and Dr. M. Knauf for their support with the expression and labeling of the *D. vulgaris* flavodoxin. All spectra were recorded at the Large Scale Facility for Biomolecular NMR at the University of Frankfurt.

REFERENCES

1. W. A. Gibbons, G. Némethy, A. Stern, and L. C. Craig, An approach to conformational analysis of peptides and proteins in solution based on a combination of nuclear magnetic resonance spectroscopy and conformational energy calculations, *Proc. Natl. Acad. Sci. USA* **67,** 239–246 (1970).
2. S. Karplus and M. Karplus, Nuclear magnetic resonance determination of the angle ψ in peptides, *Proc. Natl. Acad. Sci. USA* **69,** 3204–3206 (1972).
3. J. A. Sogn, W. A. Gibbons, and E. W. Randall, Study of nitrogen-15-labeled amino acids and peptides by nuclear magnetic resonance, *Biochemistry* **12,** 2100–2105 (1973).
4. M. Barfield and H. L. Gearhart, The conformational dependence of vicinal ^{15}N-C-C-H coupling constants in peptides, *Mol. Phys.* **27,** 899–902 (1974).
5. V. F. Bystrov, Spin-spin coupling and the conformational states of peptide systems, *Prog. Nucl. Magn. Reson. Spectrosc.* **10,** 41–81 (1976).
6. V. F. Bystrov, Y. D. Gavrilov, V. T. Ivanov, and Y. D. Ovchinnikov, Refinement of the solution conformation of valinomycin with the aid of coupling constants from the ^{13}C-nuclear-magnetic-resonance spectra, *Eur. J. Biochem.* **78,** 63–82 (1977).
7. A. DeMarco, M. Llinás, and K. Wüthrich, ^{1}H-^{15}N spin-spin couplings in alumichrome, *Biopolymers* **17,** 2727–2742 (1978).
8. K. D. Kopple, A. Ahsan, and M. Barfield, Regarding H-C-C(O)-^{15}N coupling as an indicator of peptide torsional angle, *Tetrahedron Lett.* **38,** 3519–3522 (1978).
9. A. C. Wang and A. Bax, Reparametrization of the Karplus relation for $^3J(H^\alpha$-N) and $^3J(H^N$-C′) in peptides from uniformly ^{13}C/^{15}N-enriched human ubiquitin, *J. Am. Chem. Soc.* **117,** 1810–1813 (1995).
10. G. T. Montelione, M. E. Winkler, P. Rauenbuehler, and G. Wagner, Accurate measurements of long-range heteronuclear coupling constants from homonuclear 2D NMR spectra of isotope-enriched proteins, *J. Magn. Reson.* **82,** 198–204 (1989).
11. G. Wider, D. Neri, G. Otting, and K. Wüthrich, A heteronuclear three-dimensional NMR experiment for measurements of small heteronuclear coupling constants in biological macromolecules, *J. Magn. Reson.* **85,** 426–431 (1989).
12. C. Griesinger, O. W. Sørensen, and R. R. Ernst, Correlation of connected transitions by two-dimensional NMR spectroscopy, *J. Chem. Phys.* **85,** 6837–6852 (1986).
13. A. Bax, G. W. Vuister, S. Grzesiek, F. Delaglio, A. C. Wang, R. Tschudin, and G. Zhu, Measurement of homo- and heteronuclear J couplings from quantitative J correlation, *Methods Enzymol.* **239,** 79–105 (1994).
14. S. J. Archer, M. Ikura, D. A. Torchia, and A. Bax, An alternative 3D NMR technique for correlating backbone ^{15}N with side chain Hβ resonances in larger proteins, *J. Magn. Reson.* **95,** 636–641 (1991).
15. J. C. Madsen, O. W. Sørensen, P. Sørensen, and F. M. Poulsen, Improved pulse sequences for measuring coupling constants in ^{13}C, ^{15}N-labeled proteins, *J. Biomol. NMR* **3,** 239–244 (1993).
16. P. Düx, B. Whitehead, R. Boelens, R. Kaptein, and G. W. Vuister, Measurement of ^{15}N-^{1}H coupling constants in uniformly ^{15}N-labeled proteins: Application to the photoactive yellow protein, *J. Biomol. NMR* **10,** 301–306 (1997).
17. F. Löhr, C. Pérez, J. M. Schmidt, and H. Rüterjans, Recording heteronuclear quantitative J-correlation spectra with internal reference peaks, *Bull. Magn. Reson.* **20,** 9–14 (1999).
18. M. Pellecchia, R. Fattorusso, and G. Wider, Determination of the dihedral angle ψ based on J coupling measurements in ^{15}N/^{13}C-labeled proteins, *J. Am. Chem. Soc.* **120,** 6824–6825 (1998).
19. S. Seip, J. Balbach, and H. Kessler, Determination of backbone conformation of isotopically enriched proteins based on coupling constants, *J. Magn. Reson. Ser. B* **104,** 172–179 (1994).
20. P. Permi, I. Kilpeläinen, and A. Annila, Determination of backbone angle ψ in proteins using a TROSY-based α/β-HN(CO)CA-J experiment, *J. Magn. Reson.* **146,** 255–259 (2000).
21. K. Pervushin, R. Riek, G. Wider, and K. Wüthrich, Attenuated T_2 relaxation by mutual cancellation of dipole-dipole coupling and chemical shift anisotropy indicates an avenue to NMR structures of very large biological macromolecules in solution, *Proc. Natl. Acad. Sci. USA* **94,** 12,366–12,371 (1997).
22. K. V. Pervushin, G. Wider, and K. Wüthrich, Single transition-to-single transition polarization transfer (ST2-PT) in [^{15}N,^{1}H]-TROSY, *J. Biomol. NMR* **12,** 345–348 (1998).

23. P. Andersson, A. Annila, and G. Otting, An α/β-HSQC-α/β experiment for spin-state selective editing of IS cross-peaks, *J. Magn. Reson.* **133,** 364–367 (1998).
24. J. Weigelt, Single scan, sensitivity- and gradient-enhanced TROSY for multidimensional NMR experiments, *J. Am. Chem. Soc.* **120,** 10,778–10,779 (1998).
25. M. Salzmann, G. Wider, K. Pervushin, H. Senn, and K. Wüthrich, TROSY-type triple-resonance experiments for sequential NMR assignments in large proteins, *J. Am. Chem. Soc.* **121,** 844–848 (1999).
26. A. Meissner, T. Schulte-Herbrüggen, and O. W. Sørensen, Spin-state-selective polarization or excitation for simultaneous E.COSY-type measurement of $^3J(C',H^\alpha)$ and $^3J(H^N,H^\alpha)$ coupling constants with enhanced sensitivity and resolution in multidimensional NMR spectroscopy of ^{13}C,^{15}N-labeled proteins, *J. Am. Chem. Soc.* **120,** 3803–3804 (1998).
27. A. C. Wang and A. Bax, Determination of the backbone dihedral angles ϕ in human ubiquitin from reparametrized empirical Karplus equations, *J. Am. Chem. Soc.* **118,** 2483–2494 (1996).
28. M. Görlach, M. Wittekind, B. T. Farmer II, L. E. Kay, and L. Mueller, Measurement of $^3J_{HN\alpha}$ vicinal coupling constants in proteins, *J. Magn. Reson. Ser. B* **101,** 194–197 (1993).
29. S. Grzesiek and A. Bax, The importance of not saturating H_2O in protein NMR. Application to sensitivity enhancement and NOE measurements, *J. Am. Chem. Soc.* **115,** 12,593–12,594 (1993).
30. J. Stonehouse, G. L. Shaw, J. Keeler, and E. D. Laue, Minimizing sensitivity losses in gradient-selected ^{15}N-^1H HSQC spectra of proteins, *J. Magn. Reson. Ser. A* **107,** 178–184 (1994).
31. H. Matsuo, Ē. Kupče, H. Li, and G. Wagner, Use of selective C^α pulses for improvement of HN(CA)CO-D and HN(COCA)NH-D experiments, *J. Magn. Reson. Ser. B* **111,** 194–198 (1996).
32. L. E. Kay, M. Ikura, R. Tschudin, and A. Bax, Three-dimensional triple-resonance NMR spectroscopy of isotopically enriched proteins, *J. Magn. Reson.* **89,** 496–514 (1990).
33. J. Boyd and N. Soffe, Selective excitation by pulse shaping combined with phase modulation, *J. Magn. Reson.* **85,** 406–413 (1989).
34. S. L. Patt, Single- and multiple-frequency-shifted laminar pulses, *J. Magn. Reson.* **96,** 94–102 (1992).
35. M. A. McCoy and L. Mueller, Nonresonant effects of frequency-selective pulses, *J. Magn. Reson.* **99,** 18–36 (1992).
36. Ē. Kupče and R. Freeman, Adiabatic pulses for wideband inversion and broadband decoupling, *J. Magn. Reson. Ser. A* **115,** 273–276 (1995).
37. R. Tycko, A. Pines, and R. Guckenheimer, Fixed point theory of iterative excitation schemes in NMR, *J. Chem. Phys*. **83,** 2775–2802 (1985).
38. T. M. Logan, E. T. Olejniczak, R. X. Xu, and S. W. Fesik, Side chain and backbone assignments in isotopically labeled proteins from two heteronuclear triple resonance experiments, *FEBS Lett*. **314,** 413–418 (1992).
39. S. Grzesiek and A. Bax, Amino acid type determination in the sequential assignment procedure of uniformly $^{13}C/^{15}N$-enriched proteins, *J. Biomol. NMR* **3,** 185–204 (1993).
40. K. Pervushin, R. Riek, G. Wider, and K. Wüthrich, Transverse relaxation-optimized spectroscopy (TROSY) for NMR studies of aromatic spin systems in ^{13}C-labeled proteins, *J. Am. Chem. Soc.* **120,** 6394–6400 (1998).
41. G. Zhu, X. M. Kong, X. Z. Yan, and K. H. Sze, Sensitivity enhancement in transverse relaxation optimized NMR spectroscopy, *Angew. Chem. Int. Ed. Engl*. **37**, 2859–2861 (1998).
42. D. Marion, M. Ikura, R. Tschudin, and A. Bax, Rapid recording of 2D NMR spectra without phase cycling. Application to the study of hydrogen exchange in proteins, *J. Magn. Reson.* **85,** 393–399 (1989).
43. A. Bax, R. H. Griffey, and B. L. Hawkins, Correlation of proton and nitrogen-15 chemical shifts by multiple quantum NMR, *J. Magn. Reson.* **55,** 301–315 (1983).
44. M. R. Bendall, D. T. Pegg, and D. M. Doddrell, Pulse sequences utilizing the correlated motion of coupled heteronuclei in the transverse plane of the doubly rotating frame, *J. Magn. Reson.* **52,** 81–117 (1983).
45. G. A. Morris and R. Freeman, Enhancement of nuclear magnetic resonance signals by polarization transfer, *J. Am. Chem. Soc.* **101,** 760–762 (1979).
46. J. C. Madsen and O. W. Sørensen, Multidimensional NMR experiments with improved resolution, *J. Magn. Reson.* **100,** 431–436 (1992).
47. D. R. Muhandiram, G. Y. Xu, and L. E. Kay, An enhanced-sensitivity pure absorption gradient 4D ^{15}N, ^{13}C-edited NOESY experiment, *J. Biomol. NMR* **3,** 463–470 (1993).
48. S. R. Van Doren and E. R. P. Zuiderweg, Improvements in HSMQC-type double- and triple-resonance NMR experiments by using full-sweep (semi-) constant-time shift labeling, *J. Magn. Reson. Ser. B* **104,** 193–198 (1994).
49. B. Reif, M. Hennig, and C. Griesinger, Direct measurement of angles between bond vectors in high-resolution NMR, *Science* **276**, 1230–1233 (1997).
50. D. Yang and L. E. Kay, Determination of the protein backbone dihedral angle ψ from a combination of NMR-derived cross-correlation spin relaxation rates, *J. Am. Chem. Soc.* **120,** 9880–9887 (1998).
51. P. Pelupessy, E. Chiarparin, R. Ghose, and G. Bodenhausen, Efficient determination of angles subtended by C^α-H^α and N-H^N vectors in proteins via dipole-dipole cross-correlation, *J. Biomol. NMR* **13,** 375–380 (1999).
52. R. Brüschweiler, Cross-correlation-induced *J* coupling, *Chem. Phys. Lett.* **257,** 119–122 (1996).
53. N. Tjandra, S. Grzesiek, and A. Bax, Magnetic field dependence of nitrogen-proton *J* splittings in ^{15}N-enriched human ubiquitin resulting from relaxation interference and residual dipolar coupling, *J. Am. Chem. Soc.* **118,** 6264–6272 (1996).
54. M. A. Walsh, Ph.D. Thesis, National University of Ireland (1994).
55. M. A. Walsh, A. McCarthy, P. A. O'Farrell, P. McArdle, P. D. Cunningham, S. G. Mayhew, and T. M. Higgins, X-ray crystal structure of the *Desulfovibrio vulgaris* (Hildenborough) apoflavodoxin-riboflavin complex, *Eur. J. Biochem.* **258,** 362–371 (1998).
56. R. Brüschweiler and D. A. Case, Adding harmonic motions to the Karplus relation for spin–spin coupling, *J. Am. Chem. Soc.* **116,** 11,199–11,200 (1996).
57. A. Hrovat, M. Blümel, F. Löhr, S. G. Mayhew, and H. Rüterjans, Backbone dynamics of oxidized and reduced *D. vulgaris* flavodoxin in solution, *J. Biomol. NMR* **10,** 53–62 (1997).
58. J. M. Schmidt, M. Blümel, F. Löhr, and H. Rüterjans, Self-consistent ^3J coupling analysis for the joint calibration of Karplus coefficients and evaluation of torsion angles, *J. Biomol. NMR* **14,** 1–12 (1999).
59. F. Löhr, S. G. Mayhew, and H. Rüterjans, Detection of scalar couplings across NH···OP and OH···OP hydrogen bonds in a flavoprotein, *J. Am. Chem. Soc.* **122,** 9289–9295 (2000).
60. C. Pérez, F. Löhr, H. Rüterjans, and J. M. Schmidt, Self-consistent Karplus parametrization of ^3J couplings depending on the polypeptide side-chain torsion $\chi 1$, *J. Am. Chem. Soc.* **123,** 7081–7093 (2001).
61. D. A. Case, C. Scheurer, and R. Brüschweiler, Static and dynamic effects on vicinal scalar *J* couplings in proteins and peptides: A MD/DFT analysis, *J. Am. Chem. Soc.* **112,** 10,390–10,397 (2000).
62. J. M. Schmidt, R. R. Ernst, S. Aimoto, and M. Kainosho, Determination of heteronuclear three-bond J-coupling constants in peptides by a simple heteronuclear relayed E.COSY experiment, *J. Biomol. NMR* **6,** 95–105 (1995).